RESEARCH ARTICLE

Technetium 99m–Labeled VQ Peptide: A New Imaging Agent for the Early Detection of Tumors or Premalignancies

Jiyun Shi, Liyang Cui, Bing Jia, Zhaofei Liu, Peng He, Chengyan Dong, Xiaona Jin, Huiyun Zhao, Fang Li, and Fan Wang

Abstract

There is a critical need to develop diagnostic procedures enabling early detection of tumors while at a curable stage. Technetium 99m (^{99m}Tc)-labeled VQ peptide (^{99m}Tc-HYNIC-VQ) identified through screening phage display peptide libraries against fresh human colonic adenomas was prepared and evaluated for tumor detection. ^{99m}Tc-HYNIC-VQ was prepared by a non-$SnCl_2$ method with more than 99% radiochemical purity. The biodistribution in the HT-29 tumor model showed that although the absolute tumor uptake values were relatively low (0.60 ± 0.09, 0.41 ± 0.09, 0.36 ± 0.18, and 0.19 ± 0.08 %ID/g at 0.5, 1, 2, and 4 hours postinjection, respectively), the tumor uptake was higher than that of any of the other organs except for the kidneys at any time point examined, which led to the high tumor to nontarget ratios. The tumors and inflammation were clearly visualized with high contrast. Although the mechanism of accumulation of radiolabeled VQ peptide in tumors and inflammation needs to be further investigated, ^{99m}Tc-HYNIC-VQ is a promising imaging agent for the early detection of tumors or premalignancies, at least for screening patients with a high risk of developing cancers.

MOLECULAR IMAGING is often defined as the visualization, characterization, and measurement of biologic processes at the molecular and cellular levels in humans and other living systems.[1] By noninvasively characterizing tumor biology, molecular imaging is now playing an indispensable role in tumor diagnosis, therapy monitoring, and prognostic evaluation. Among all the imaging modalities, optical imaging, positron emission tomography (PET), and single-photon emission computed tomography (SPECT) stand out because of their high sensitivity. PET and SPECT are commonly used in routine clinical practice and trials.[2–7]

Colorectal cancer is the third most common cancer in the United States, causing nearly 1 in 10 cancer-related deaths.[8] This high incidence results from the limitations of conventional endoscopic screening, which reveals only anatomic changes.[9] Moreover, flat lesions or lesions originating either from polyposis syndromes or from inflammatory bowel diseases are usually missed by routine endoscopy, which significantly retards the early detection of premalignant lesions and the effective prevention of this disease.[10–13] Therefore, it is urgent to develop new methods to identify high-risk individuals and detect early changes in the population. A number of biomarkers involved in the physiologic or pathologic events in carcinogenesis and subsequent development of cancer are under investigation to be the targets for early detection.[14,15] Although less specific when compared to antibodies to these biomarkers, peptides are typically less immunogenic, are much easier to penetrate into tissues and clear rapidly from the blood, and are more convenient to produce.[16] The identification and optimization of tumor biomarker–targeted peptides guarantee a new approach to developing probes for tumor detection and staging.

Recently, a series of reports regarding peptides identified from phage display have shown proof of principle that certain cancer-specific phage library–derived probes can be developed for the detection of premalignant

From the Medical Isotopes Research Center, Medical and Healthy Analytical Center, and Department of Radiation Medicine, School of Basic Medical Sciences, Peking University, Beijing, China; and the Department of Nuclear Medicine, Peking Union Medical College Hospital, Beijing, China.

Address reprint requests to: Fan Wang PhD, Medical Isotopes Research Center, Peking University, 38# Xueyuan Road, Beijing 100191, China; e-mail: wangfan@bjmu.edu.cn.

DOI 10.2310/7290.2012.00047

© *2013 Decker Publishing*

DECKER

tissues and solid tumors at an early stage by optical means.[17–19] VRPMPLQ (Val-Arg-Pro-Met-Pro-Leu-Gln [VQ]) is a heptapeptide sequence first identified by Hsiung and colleagues by screening phage display peptide libraries against fresh human colonic adenomas.[20] In vitro studies showed that binding of VQ peptide to HT-29 human colon cells was around 20-fold greater than its binding to Hs738.st/int nonmalignant human intestinal cells. In vivo studies indicated that the fluorescein-conjugated VQ peptide bound more strongly to dysplastic colonocytes than to adjacent normal cells in the same subject. It is suggested that VQ is a promising targeting molecule of probes for the early detection of colorectal cancer and potentially of other epithelial malignancies.

In this study, we present the synthesis and evaluation of ^{99m}Tc-HYNIC-VQ (HYNIC = 6-hydrazinonicotinamide) as a SPECT radiotracer for tumor imaging in five different xenografted tumor-bearing animal models (HT-29 human colon cancer, CL187 human colon cancer, BGC823 human gastric cancer, U87MG human glioma, and UM-SCC-22B human head and neck cancer). These tumors were clearly visualized with high contrast. Given that patients with chronic inflammatory bowel disease are at increased risk for developing malignancy due to undetected dysplastic lesions,[11] and that the mediators and cellular effectors of inflammation are important constituents of the local environment of tumors,[21] we subsequently explored the capability of ^{99m}Tc-HYNIC-VQ to image inflammation. The main objective of this study was to assess the potential of ^{99m}Tc-HYNIC-VQ for the early detection of tumors or premalignancies.

Materials and Methods

All commercially available chemical reagents were of analytic grade and used without further purification. Trisodium triphenylphosphine-3,3′,3′′-trisulfonate (TPPTS) and tricine were purchased from Sigma-Aldrich (St. Louis, MO). HYNIC-VQ peptide and HYNIC-QV peptide, QLMRPPV (Gln-Leu-Met-Arg-Pro-Pro-Val [QV], a scrambled peptide), were custom-made by GL Biochem (Shanghai) Ltd. $Na^{99m}TcO_4$ was obtained from a commercial ^{99}Mo/^{99m}Tc generator (Beijing Atom High Tech Co., Ltd., Beijing, China).

Cell Culture

The BGC823 human gastric cancer cells were kindly provided by Dr. Yang (Peking University School of Oncology). UM-SCC-22B human head and neck cancer cells were kindly provided by Dr. Chen (National Institute of Biomedical Imaging and Bioengineering). The HT-29 and CL187 human colon cancer cells and U87MG human glioma cells were purchased from ATCC (Manassas, VA). BGC823, HT-29, CL187, and UM-SCC-22B cells were cultured in high-glucose Dulbecco's Modified Eagle's Medium (DMEM), whereas U87MG cells were cultured in low-glucose DMEM. All cell lines were cultured in medium supplemented with 10% (v/v) fetal bovine serum at 37°C in a humidified atmosphere with 5% CO_2.

Preparation of ^{99m}Tc-HYNIC-VQ

To a clean vial was added 100 μL of HYNIC-VQ solution (100 μg/mL in water), 100 μL of tricine solution (100 mg/mL in 25 mM succinate buffer, pH 5.0), 100 μL of TPPTS solution (50 mg/mL in 25 mM succinate buffer, pH 5.0), and 100 μL of $Na^{99m}TcO_4$ (370–1,110 MBq). The reaction mixture was heated at 100°C for 20 minutes. After radiolabeling, a sample of the resulting solution was analyzed by radio–high-performance liquid chromatography (HPLC). As a control peptide, ^{99m}Tc-HYNIC-QV was prepared as above.

The radio-HPLC method used a HP Hewlett Packard Series 1100 HPLC system equipped with Radioflow Detector LB509 and an Agilent Zorbax SB-C18 column (4.6 mm × 250 mm, 5 μm). The flow rate was 1.0 mL/min. The mobile phase was isocratic with 100% solvent A (0.05% trifluoroacetic acid [TFA] in water) and 0% solvent B (0.05% TFA in acetonitrile) at 0 to 3 minutes, followed by a gradient mobile phase going from 0% solvent B at 3 minutes to 25% solvent B at 5 to 18 minutes and to 70% solvent B at 22 minutes, then to 0% solvent B at 24 to 30 minutes.

Dose Preparation for Animal Studies

The ^{99m}Tc-HYNIC-VQ and ^{99m}Tc-HYNIC-QV were purified using a Sep-Pak C-18 cartridge (Waters Corp., Milford, MA) before animal studies. The Sep-Pak C-18 cartridge was activated with ethanol (10 mL) and was washed with water (10 mL). After the radiotracer was loaded, the Sep-Pak C-18 cartridge was washed with saline (10 mL) to remove the unlabeled ^{99m}Tc and excess coligands. The radiotracer was eluted with 80% ethanol (0.4 mL). Doses for animal studies were prepared by dissolving the purified radiotracer in saline to give a concentration of ≈ 3.7 MBq/mL (≈ 0.2 μg peptide) for biodistribution studies and ≈ 74 MBq/mL (≈ 4 μg peptide) for imaging studies.

Animal Models

Female BALB/c nude mice and normal BALB/c mice (4–5 weeks of age) were purchased from the Department of Laboratory Animal Science, Peking University Health Science Center. All animal experiments were performed in accordance with the guidelines of the Institutional Animal Care and Use Committee at Peking University. The cancer cells (5×10^6) were implanted subcutaneously into the right or left upper flanks of nude mice. When tumors reached $\approx$ 0.8 cm in mean diameter, the tumor-bearing mice were used in biodistribution and imaging studies. As for the inflammation model, turpentine (0.1 mL/mouse) was injected subcutaneously into the suprascapular region on the normal BALB/c mice.[22] The different animal models are summarized in Table S1 (online version only) for imaging with different radiotracers.

Biodistribution

Sixteen HT-29 tumor–bearing nude mice were randomly divided into four groups, each of which had four animals. The ^{99m}Tc radiotracer ($\approx$ 370 kBq or $\approx$ 10 μCi in 0.1 mL saline) was administered intravenously to each tumor-bearing mouse. Animals were anesthetized with intraperitoneal injection of sodium pentobarbital at a dose of 45.0 mg/kg. Animals were sacrificed by cervical dislocation 0.5, 1, 2, and 4 hours postinjection. Blood, heart, liver, spleen, kidney, lung, stomach, intestine, muscle, and tumor were harvested, weighed, and measured for radioactivity in a gamma-counter (Wallac 1470-002, PerkinElmer, Turku, Finland). The organ uptake was calculated as the percentage of injected dose per gram of wet tissue mass (%ID/g). The biodistribution study of ^{99m}Tc-HYNIC-VQ in the inflammation model was performed using the same procedure. The biodistribution data and target to nontarget (T/NT) ratios are reported as an average plus the standard deviation.

Scintigraphic Imaging

Planar imaging studies were performed on three BALB/c nude mice bearing HT-29 human colon cancer xenografts. Animals were anesthetized with intraperitoneal injection of sodium pentobarbital at a dose of 45.0 mg/kg. Each tumor-bearing mouse was administered $\approx$ 14.8 MBq of ^{99m}Tc-HYNIC-VQ dissolved in 0.2 mL of saline. Animals were placed supine on a two-head gamma-camera (Millennium VG, GE) equipped with a parallel-hole, low-energy, high-resolution collimator. Anterior images were acquired 1 and 2 hours postinjection and stored digitally in a 128 $\times$ 128 matrix. The acquisition count limits were set at 200 kilo counts. The imaging studies were also performed on a CL187 human colon cancer model, a BGC823 human gastric cancer model, a UM-SCC-22B human head and neck cancer model, and a U87MG human glioma model, as well as an inflammation model, using the same procedure above.

Specificity Study

We carried out the in vitro assessment first. For the binding assay, HT-29 and CL187 colon cancer cells (2×10^5 per well) were incubated separately with $\approx$ 200,000 cpm of ^{99m}Tc-HYNIC-VQ for 2 hours at 4°C with or without blocking solution (excess HYNIC-VQ) in Millipore 24-well plates (Millipore Corp., Billerica, MA). Incubation was interrupted by rapid rinsing with ice-cold 0.1 M PBS (pH 7.4) buffer to remove the free radioactivity. The bound activity was collected by solubilized cells with 2 M NaOH and then measured in a gamma-counter (Wallac 1470-002). The results are expressed as the percentage of the bound radioactivity versus totally added radioactivity after decay correction. All experiments were carried out twice with quadruple samples for each.

For the in vivo studies, four HT-29 tumor–bearing nude mice were used for the blocking experiment. Each animal was coinjected with 300 μg of HYNIC-VQ and ^{99m}Tc-HYNIC-VQ. One hour postinjection, all four animals were sacrificed for biodistribution using the same procedure as above. The results were compared to those obtained from animals without the injection of excess HYNIC-VQ. The biodistribution of ^{99m}Tc-HYNIC-QV in an HT-29 tumor model and the imaging of ^{99m}Tc-HYNIC-QV on tumor and inflammation models were also performed using the same procedure outlined above.

Statistical Analysis

Quantitative data are expressed as mean $\pm$ SD. Means were compared using one-way analysis of variance (ANOVA) and the Student *t*-test; p values $< .05$ were considered statistically significant.

Results

Radiochemistry

^{99m}Tc-HYNIC-VQ/QV was prepared using a non-$SnCl_2$ one-step procedure.[23–26] HYNIC-VQ/QV was allowed to

react with $Na^{99m}TcO_4$ in the presence of excess tricine and TPPTS to form the ternary ligand complex ^{99m}Tc(HYNIC-VQ/QV)(tricine)(TPPTS). The radiolabeling yield was $>$ 95%, and the specific activity was $\approx$ 1,000 mCi/μmol. The radiochemical purity was $>$ 99% after purification with the Sep-Pak C-18 cartridge. The HPLC retention time for ^{99m}Tc-HYNIC-VQ was 9.8 minutes (Figure 1).

Biodistribution Characteristics

A biodistribution study was performed using female BALB/c nude mice bearing the HT-29 human colon cancer xenografts. The selected biodistribution data and T/NT ratios for ^{99m}Tc-HYNIC-VQ are summarized in Figure 2. In general, rapid distribution and clearance were observed, especially between 0.5 and 1 hour postinjection. ^{99m}Tc-HYNIC-VQ had the highest tumor uptake (0.60 $\pm$ 0.09 %ID/g) at 0.5 hours postinjection. Although the absolute tumor uptake values were relatively low (0.60 $\pm$ 0.09, 0.41 $\pm$ 0.09, 0.36 $\pm$ 0.18, and 0.19 $\pm$ 0.08 %ID/g at 0.5, 1, 2, and 4 hours postinjection, respectively), the tumor uptake was higher than that of any of the other organs except for the kidneys at any time point examined, which led to the high T/NT ratios. Almost all T/NT values were more than 21 hour postinjection, and the highest T/NT ratios were reached at 2 hours postinjection, with 5.94 $\pm$ 1.51 for tumor to blood, 3.33 $\pm$ 0.58 for tumor to liver, and 9.14 $\pm$ 3.17 for tumor to muscle. The high T/NT ratios guaranteed images with good contrast. The biodistribution data of ^{99m}Tc-HYNIC-VQ in the inflammation model are summarized in Figure S1 (online version only). The inflammation uptake at 1 hour postinjection was 0.35 $\pm$ 0.06 %ID/g, similar to the tumor uptake in the HT-29 tumor model ($p > .05$). There were no significant differences between T/NT ratios of ^{99m}Tc-HYNIC-VQ in the HT-29 tumor model and the inflammation model.

Scintigraphic Imaging

Imaging studies were first performed in the BALB/c nude mice bearing HT-29 human colon cancer xenografts. Figure 3 illustrates representative scintigraphic images of tumor-bearing mice administered with $\approx$ 14.8 MBq of ^{99m}Tc-HYNIC-VQ. The tumors were clearly visualized at 1 hour postinjection with excellent tumor to background contrast. The ''hottest'' spots were the tumor, kidneys, and bladder. The high uptake in the kidneys and bladder confirmed the excretion of this tracer through the renal route. By 2 hours postinjection, the tumors were still clearly visible with a high contrast to the background.

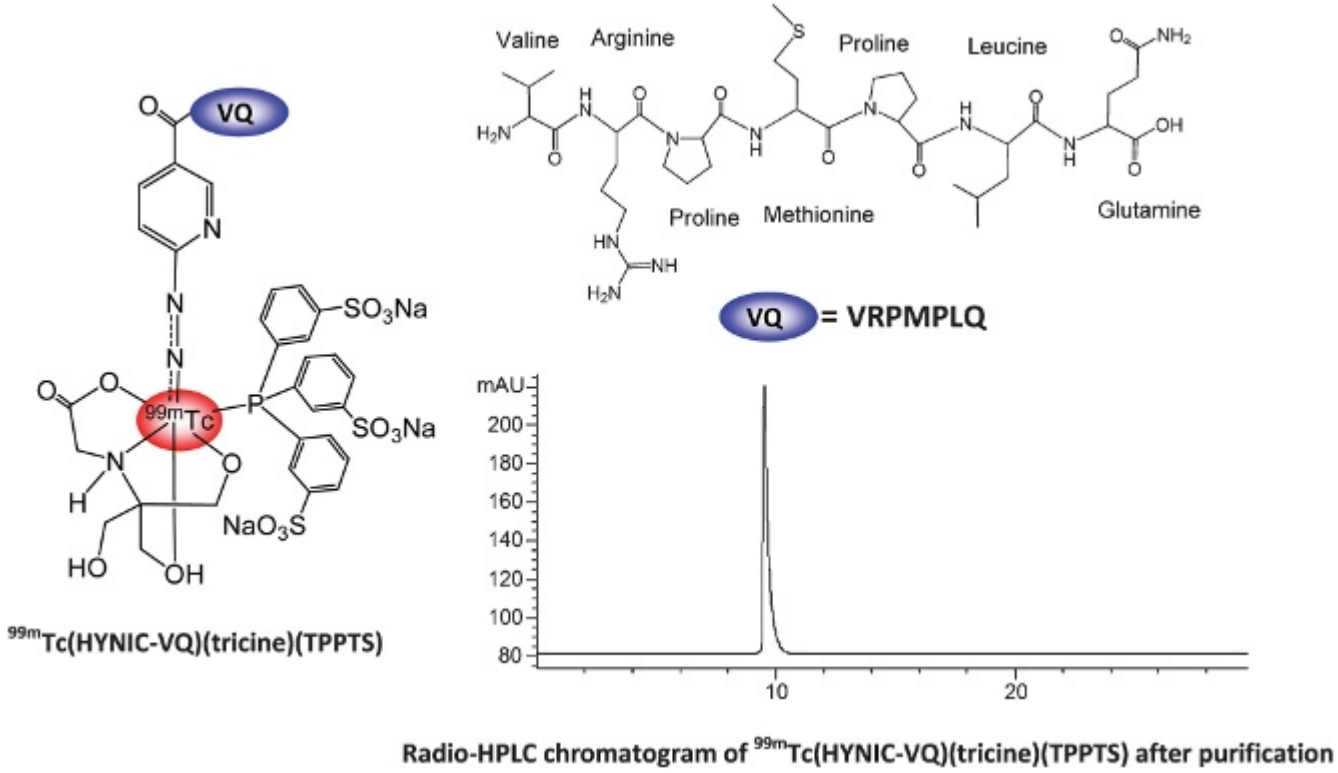

Figure 1. Structure and radio-HPLC chromatogram of ^{99m}Tc-HYNIC-VQ.

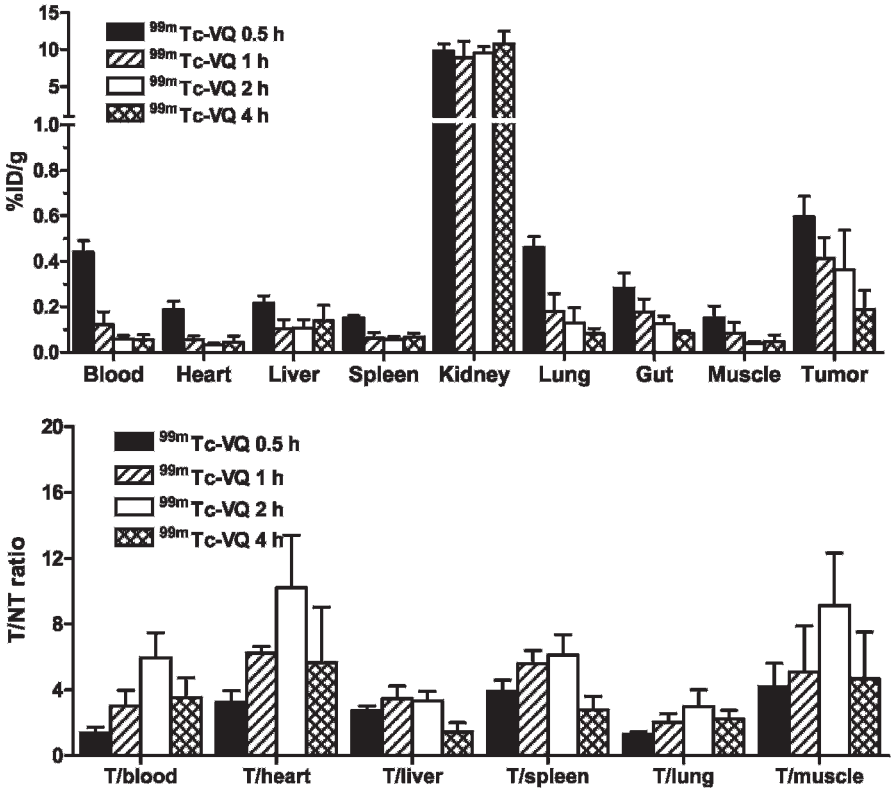

Figure 2. Biodistribution data (*top*) and tumor to nontarget (T/NT) ratios (*bottom*) for ^{99m}Tc-HYNIC-VQ (≈ 370 kBq per mouse) in BALB/c nude mice bearing HT-29 colon cancer xenografts. Data are expressed as mean ± SD, $n = 4$.

These data were completely consistent with those obtained from the ex vivo biodistribution study (see Figure 2).

The CL187 colon cancer model and the BGC823 gastric cancer model were also used to evaluate radiolabeled VQ peptide as a radiotracer for the imaging of gastrointestinal cancers. Tumors were clearly visualized in both two tumor models at 1 hour postinjection (Figure 4). Subsequently, we tested ^{99m}Tc-HYNIC-VQ in the UM-SCC-22B head and neck cancer model and the U87MG glioma model. Similar results were achieved as shown in Figure 4. With respect to the inflammation imaging, the inflammation areas in normal mice also could be visualized at 1 and 2 hours postinjection (Figure 5). The imaging results suggested that VQ peptide might be correlative with cancer-related inflammation other than cell surface receptors.

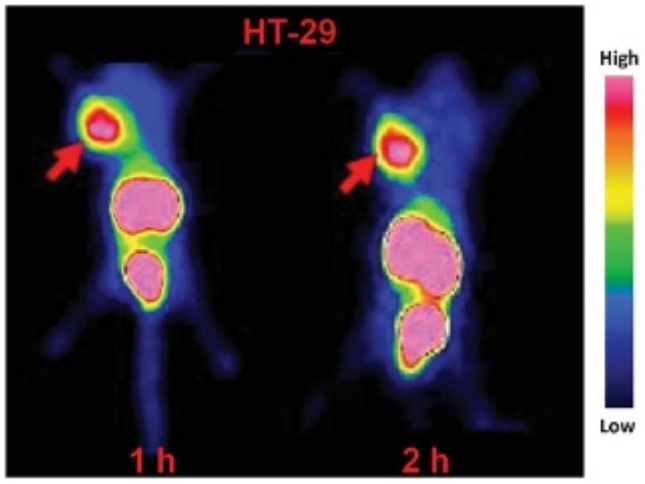

Figure 3. Static planar images of nude mice bearing HT-29 colon cancer xenografts 1 and 2 hours after injection of ≈ 14.8 MBq of ^{99m}Tc-HYNIC-VQ. The *arrows* indicate the presence of tumors.

Specificity Study

Figure 6A shows the results of ^{99m}Tc-HYNIC-VQ binding to HT-29 and CL187 colon cancer cells. A very low radioactivity was bound to both two tumor cells, and there were no significant differences with and without the excess cold peptide (0.38 ± 0.04 vs 0.45 ± 0.13 for HT-29 cells, 0.55 ± 0.03 vs 0.57 ± 0.05 for CL187 cells, $p > .05$). This further confirmed that ^{99m}Tc-HYNIC-VQ did not bind specifically to some receptors on the surface of tumor cells.

In the blocking experiment (Figure 6B), the coinjection of HYNIC-VQ did not induce the reduced tumor uptake of ^{99m}Tc-HYNIC-VQ, whereas the tumor uptake increased appreciably (0.43 ± 0.19 %ID/g vs 0.55 ± 0.13 %ID/g, $p > .05$). This result indicated that the

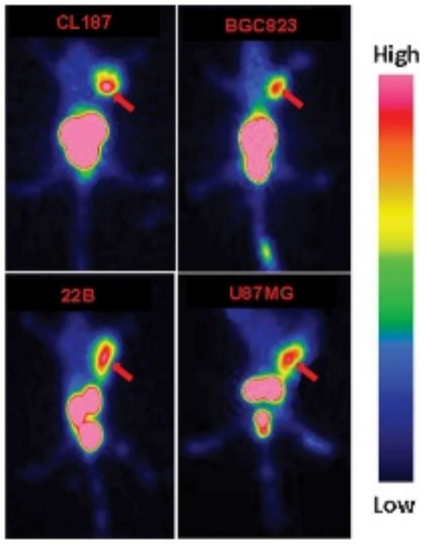

Figure 4. Static planar images of nude mice bearing the different cancer xenografts 1 hour after injection of ≈ 14.8 MBq of ^{99m}Tc-HYNIC-VQ. The *arrows* indicate the presence of tumors.

accumulation of ^{99m}Tc-HYNIC-VQ in tumors was not mediated by receptors on the tumor cell surface.

Figure 6, C and D, shows the biodistribution data of ^{99m}Tc-HYNIC-QV in the HT-29 tumor model at 1 hour postinjection. The tumor uptake was 0.44 ± 0.09 %ID/g, similar to 0.41 ± 0.09 %ID/g of ^{99m}Tc-HYNIC-VQ ($p > .05$). The T/NT ratios were higher than those of ^{99m}Tc-HYNIC-VQ ($p < .05$ for tumor to blood, tumor to heart, tumor to spleen, and tumor to muscle).

The representative images of ^{99m}Tc-HYNIC-QV in the HT-29 colon cancer model, BGC823 gastric cancer model, UM-SCC-22B head and neck cancer model, and

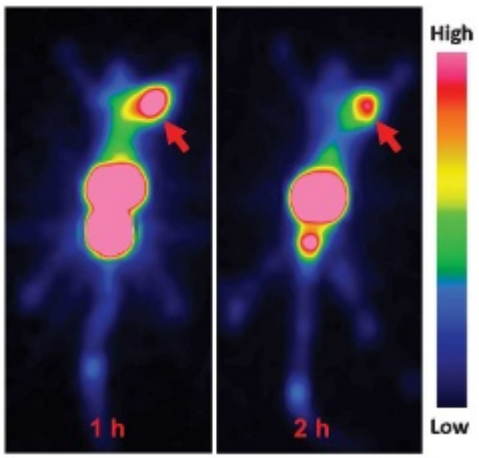

Figure 5. Static planar images of the inflammation mouse model 1 and 2 hours after injection of ≈ 14.8 MBq of ^{99m}Tc-HYNIC-VQ. The *arrows* indicate the presence of inflammation.

inflammation model are shown in Figure S2 (online version only). The tumors and the inflammation area are clearly visualized.

Discussion

A major goal of molecular imaging is guiding the early assessment, risk stratification, evaluation, and follow-up of patients.[1] Regular probes that can bind to the specific targets are more favorable because of the accurate delineation of cancer biologic processes. However, some molecules, which are able to evaluate complex biologic processes without targeting specific biomarkers, are now under intense investigation and assisting clinicians in orienting toward different adjustments of therapy. One paradigm is the ^{99m}Tc-labeled lipophilic cation ^{99m}Tc-MIBI, in particular.[27] Different parameters of ^{99m}Tc-MIBI from single- or multimodality scanning can provide information from various angles, including cellular process and function, the activity of drug transporters, and multidrug resistance in a variety of malignant tumors.[28–31]

The VQ peptide was identified by screening phage display peptide libraries against fresh human colonic adenomas, with preferential binding to premalignant tissue.[20] Although the molecular target of the VQ peptide is unknown, previous research by Hsiung and colleagues showed that the fluorescein-conjugated VQ peptide selectively binds to dysplastic tissue over normal mucosa, which enables the detection of premalignancies.[20] In addition, this VQ peptide was discovered through intact tissue panning, which might have the advantage of selecting for targets that are not differentially expressed but are clinically relevant because of accessibility.

Currently, nuclear imaging is one of the most widely used modalities in the clinic. In this research, we primarily focused on investigating the capacity of radiolabeled VQ as a radiotracer for the SPECT imaging of tumors. ^{99m}Tc is the most common SPECT radioisotope for clinical use, with easy availability and a low price. For the ^{99m}Tc labeling, we chose HYNIC as the bifunctional chelator and tricine/TPPTS as coligands to form the ternary ligand complex with favorable properties of stability and pharmacokinetics.[32] Since the VQ peptide was identified from the fresh human colonic adenomas, we first tested ^{99m}Tc-HYNIC-VQ in the HT-29 human colon cancer model. One important characteristic of any imaging probe is its uptake efficiency at tumor sites and its lack of accumulation at nontumor sites. The biodistribution data revealed that although the absolute uptake of ^{99m}Tc-HYNIC-VQ in tumor was relatively low, it was higher than

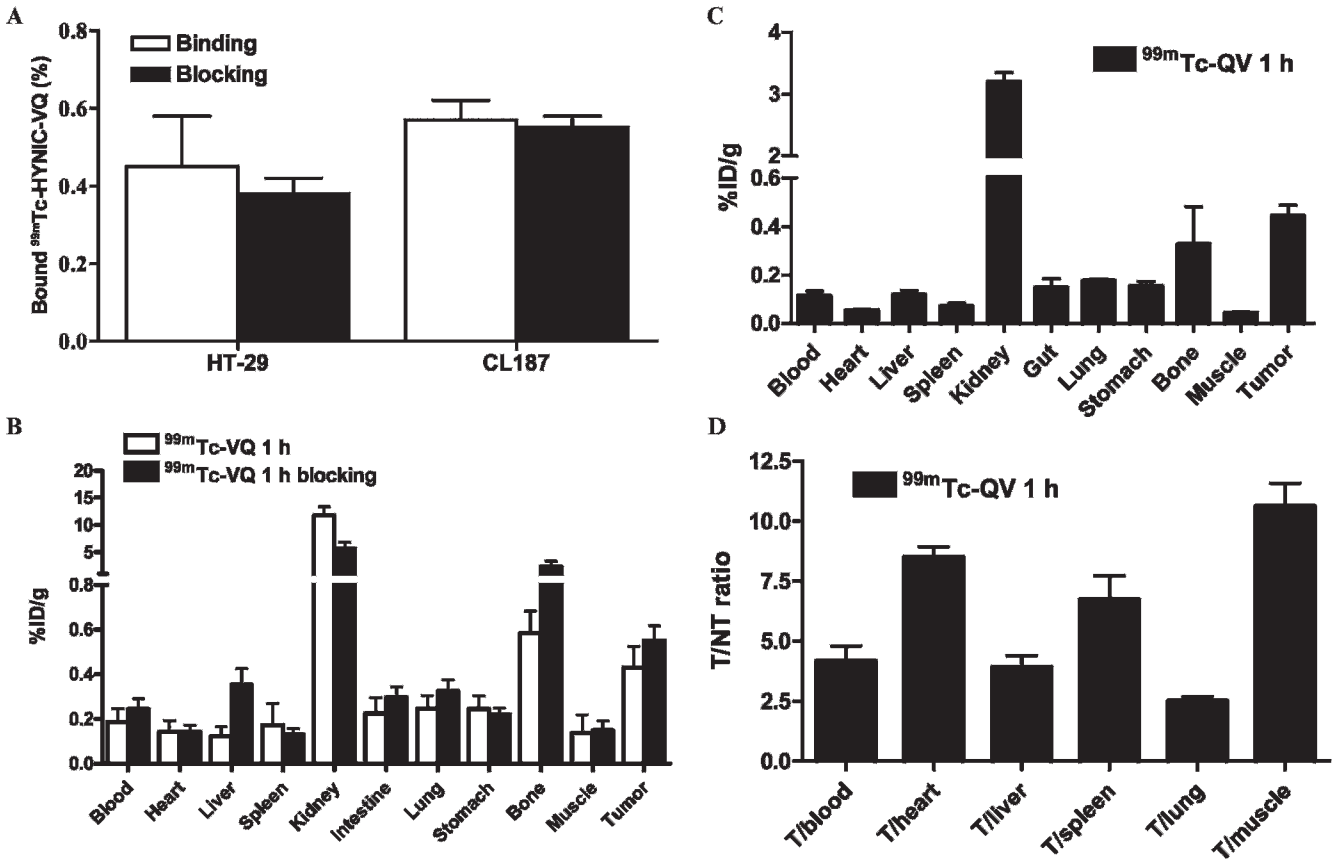

Figure 6. Binding of ^{99m}Tc-HYNIC-VQ to HT-29 and CL187 human colon cancer cells with or without blocking with excess HYNIC-VQ (A). Blocking experiment for ^{99m}Tc-HYNIC-VQ (≈ 370 kBq per mouse) in BALB/c nude mice bearing HT-29 colon cancer xenografts (B). Biodistribution data (C) and tumor to nontarget (T/NT) ratios (D) for ^{99m}Tc-HYNIC-QV (≈ 370 kBq per mouse) in BALB/c nude mice bearing HT-29 colon cancer xenografts. Data are expressed as mean ± SD, $n = 4$.

in other normal organs, except for the kidneys (see Figure 2). This result, on the one hand, warrants high-contrast imaging of tumors; on the other hand, it minimizes the radiation exposure to normal organs. The gamma images show that tumor, kidneys, and bladder are clearly visible due to the much lower background signal of the whole body (see Figure 3). It has been reported that using the T/NT ratio improves the sensitivity of nuclear medicine imaging for the diagnosis of small lesions.[33] The aforementioned data justify the further validating of ^{99m}Tc-HYNIC-VQ in other tumor models.

To substantiate the efficacy of ^{99m}Tc-HYNIC-VQ in imaging gastrointestinal tumors, we applied this tracer to CL187 human colon cancer and BGC823 human gastric cancer models. The tumors were also clearly visualized (see Figure 4). Hsiung and colleagues reported that the VQ sequence might be promising for the early detection of colorectal cancer and potentially of other epithelial malignancies,[20] so U87MG human glioma and UM-SCC-22B human head and neck cancer models were used for the imaging of ^{99m}Tc-HYNIC-VQ, and similar results were achieved (see Figure 4). We supposed that there must be a mutual mechanism for the imaging of ^{99m}Tc-HYNIC-VQ in different tumor models.

The link between cancer and inflammation was first postulated in the nineteenth century, and it was later proven by epidemiologic studies that chronic inflammation predisposed individuals to various types of cancer.[34] Many triggers of chronic inflammation were also inclined to elevate the risk of carcinogenesis.[35] It is difficult to make an animal model with premalignancy. Given the relativity between cancer and inflammation, we made an inflammation model and performed the biodistribution and imaging experiments with ^{99m}Tc-HYNIC-VQ. The uptake of inflammation and normal organs was similar to that in the HT-29 tumor model (see Figure S1), and the inflammatory areas were clearly imaged (see Figure 5). All of these results imply that the accumulation of ^{99m}Tc-HYNIC-VQ is correlative with inflammation factors, not some receptors expressed on the surface of tumor cells.

Cell binding studies showed that there were no significant differences with and without the excess cold peptide for ^{99m}Tc-HYNIC-VQ binding to HT-29 and CL187 human colon cancer cells (see Figure 6A). The blocking experiment in the HT-29 human colon cancer model also showed that coinjection of excess cold peptide did not reduce the accumulation of ^{99m}Tc-HYNIC-VQ in tumors (see Figure 6B). As a control, ^{99m}Tc-HYNIC-QV showed similar tumor uptake and high-contrast images in tumor and inflammation models (see Figure 6C and Figure S2). To verify if any ^{99m}Tc-labeled peptide has this property, we performed the imaging studies with the ^{99m}Tc-labeled peptide octreotide (^{99m}Tc-TOC) in the HT-29 human colon cancer model, the BGC823 human gastric cancer model, and the U87MG human glioma model. As shown in Figure S3 (online version only), the imaging results were negative. This result revealed that even though the accumulation of ^{99m}Tc-HYNIC-VQ/QV in tumors and inflammation was induced by vascular permeability, there must be a mechanism. Perhaps the assembly of two or three amino acids among the seven amino acids played an important role.

There is a critical need to develop diagnostic procedures enabling early detection of tumors while at a curable stage. Hsiung and colleagues identified the VQ peptide targeting dysplasia in a clinically relevant setting, and a pilot study in patients undergoing routine colonoscopy validated that the fluorescein-conjugated VQ peptide preferentially bound to premalignant tissue.[20] Our research work demonstrated that ^{99m}Tc-labeled VQ peptide could clearly visualize tumors and inflammation in animal models. As mentioned above, the specific agents are favorable, but the nonspecific agents also have clinical values. The excellent biodistribution and high-contrast image of ^{99m}Tc-HYNIC-VQ merit further investigation to see if these findings can be translated to the clinical setting. Therefore radiolabeled VQ peptide is promising for screening patients with a high risk of developing cancers. Further studies will also be needed to understand the mechanism of accumulation of radiolabeled VQ peptide in tumors and inflammation.

Conclusion

We prepared ^{99m}Tc-HYNIC-VQ by a non-$SnCl_2$ method with more than 99% radiochemical purity. The in vivo studies showed the high-contrast images of ^{99m}Tc-HYNIC-VQ in different tumor models and an inflammation model. Although the mechanism of accumulation of radiolabeled VQ peptide in tumors and inflammation needs to be further investigated, ^{99m}Tc-HYNIC-VQ is a promising imaging agent for the early detection of tumors or premalignancies, at least for screening patients with a high risk of developing cancers. To the best of our knowledge, this is the first preclinical investigation of radiolabeled VQ peptide for tumor detection.

Acknowledgments

We thank Dr. Yang and Dr. Chen for providing the BGC823 human gastric cancer cells and the UM-SCC-22B human head and neck cancer cells.

Financial disclosure of authors: This work was financially supported in part by the Outstanding Youth Fund (81125011), "973" projects (2011CB707703 and 2013CB733802), National Natural Science Foundation of China (NSFC) projects (81000625, 30930030, 81222019, 30900373, 81201127, and 81028009), grants from the Ministry of Science and Technology of China (2011YQ030114, 2012ZX09102301-018, and 2012BAK25B03-16), and grants from the Ministry of Education of China (31300 and BMU20110263).

References

1. Mankoff DA. A definition of molecular imaging. J Nucl Med 2007;48:18N, 21N.
2. Weissleder R, Pittet MJ. Imaging in the era of molecular oncology. Nature 2008;452:580–9, doi:10.1038/nature06917.
3. Schober O, Rahbar K, Riemann B. Multimodality molecular imaging—from target description to clinical studies. Eur J Nucl Med Mol Imaging 2009;36:302–14, doi:10.1007/s00259-008-1042-4.
4. Brindle K. New approaches for imaging tumour responses to treatment. Nat Rev Cancer 2008;8:94–107, doi:10.1038/nrc2289.
5. Quon A, Gambhir SS. FDG-PET and beyond: molecular breast cancer imaging. J Clin Oncol 2005;23:1664–73, doi:10.1200/JCO.2005.11.024.
6. Neves AA, Brindle KM. Assessing responses to cancer therapy using molecular imaging. Biochim Biophys Acta 2006;1766:242–61.
7. Kelloff GJ, Krohn KA, Larson SM, et al. The progress and promise of molecular imaging probes in oncologic drug development. Clin Cancer Res 2005;11:7967–85, doi:10.1158/1078-0432.CCR-05-1302.
8. Jemal A, Siegel R, Ward E, et al. Cancer statistics, 2007. CA Cancer J Clin 2007;57:43–66, doi:10.3322/canjclin.57.1.43.
9. Winawer SJ, Zauber AG, Ho MN, et al. Prevention of colorectal cancer by colonoscopic polypectomy. The National Polyp Study Workgroup. N Engl J Med 1993;329:1977–81, doi:10.1056/NEJM199312303292701.
10. Kudo S, Kashida H, Tamura T, et al. Colonoscopic diagnosis and management of nonpolypoid early colorectal cancer. World J Surg 2000;24:1081–90, doi:10.1007/s002680010154.
11. Mayer R, Wong WD, Rothenberger DA, et al. Colorectal cancer in inflammatory bowel disease: a continuing problem. Dis Colon Rectum 1999;42:343–7, doi:10.1007/BF02236351.
12. Muto T, Bussey HJ, Morson BC. The evolution of cancer of the colon and rectum. Cancer 1975;36:2251–70, doi:10.1002/cncr.2820360944.

13. Rex DK, Cutler CS, Lemmel GT, et al. Colonoscopic miss rates of adenomas determined by back-to-back colonoscopies. Gastroenterology 1997;112:24–8, doi:10.1016/S0016-5085(97)70214-2.
14. Kelloff GJ, Sigman CC, Johnson KM, et al. Perspectives on surrogate end points in the development of drugs that reduce the risk of cancer. Cancer Epidemiol Biomarkers Prev 2000;9:127–37.
15. Garcea G, Sharma RA, Dennison A, et al. Molecular biomarkers of colorectal carcinogenesis and their role in surveillance and early intervention. Eur J Cancer 2003;39:1041–52, doi:10.1016/S0959-8049(03)00027-3.
16. Okarvi SM. Peptide-based radiopharmaceuticals: future tools for diagnostic imaging of cancers and other diseases. Med Res Rev 2004;24:357–97, doi:10.1002/med.20002.
17. Kelly K, Alencar H, Funovics M, et al. Detection of invasive colon cancer using a novel, targeted, library-derived fluorescent peptide. Cancer Res 2004;64:6247–51, doi:10.1158/0008-5472.CAN-04-0817.
18. Abraham JM, Sato F, Cheng Y, et al. Novel decapeptides that bind avidly and deliver radioisotope to colon cancer cells. PLoS One 2007;2:e964, doi:10.1371/journal.pone.0000964.
19. Lee SM, Lee EJ, Hong HY, et al. Targeting bladder tumor cells in vivo and in the urine with a peptide identified by phage display. Mol Cancer Res 2007;5:11–9, doi:10.1158/1541-7786.MCR-06-0069.
20. Hsiung PL, Hardy J, Friedland S, et al. Detection of colonic dysplasia in vivo using a targeted heptapeptide and confocal microendoscopy. Nat Med 2008;14:454–8, doi:10.1038/nm1692.
21. Mantovani A, Allavena P, Sica A, et al. Cancer-related inflammation. Nature 2008;454:436–44, doi:10.1038/nature07205.
22. Robinson GB. The catabolism of plasma glycoproteins in normal and injured rats. Biochem J 1969;114:635–40.
23. Liu S, Edwards DS, Ziegler MC, et al. 99mTc-labeling of a hydrazinonicotinamide-conjugated vitronectin receptor antagonist useful for imaging tumors. Bioconjug Chem 2001;12:624–9, doi:10.1021/bc010012p.
24. Liu S, Edwards DS, Harris AR, et al. Towards developing a non-SnCl2 formulation for RP444, a new radiopharmaceutical for thrombus imaging. J Pharm Sci 2001;90:114–23, doi:10.1002/1520-6017(200102)90:2<114::AID-JPS2>3.0.CO;2-0.
25. Wang L, Shi J, Kim YS, et al. Improving tumor-targeting capability and pharmacokinetics of (99m)Tc-labeled cyclic RGD dimers with PEG(4) linkers. Mol Pharm 2009;6:231–45, doi:10.1021/mp800150r.
26. Liu Z, Jia B, Shi J, et al. Tumor uptake of the RGD dimeric probe (99m)Tc-G(3)-2P(4)-RGD2 is correlated with integrin alpha(v)-beta(3) expressed on both tumor cells and neovasculature. Bioconjug Chem 2010;21:548–55, doi:10.1021/bc900547d.
27. Mariani G. Unexpected keys in cell biochemistry imaging: some lessons from technetium-99m-sestamibi. J Nucl Med 1996;37:536–8.
28. Del Vecchio S, Zannetti A, Aloj L, et al. Inhibition of early 99mTc-MIBI uptake by Bcl-2 anti-apoptotic protein overexpression in untreated breast carcinoma. Eur J Nucl Med Mol Imaging 2003;30:879–87, doi:10.1007/s00259-003-1161-x.
29. Zhu X, Wu H, Xia J, et al. The relationship between (99m)Tc-MIBI uptakes and tumor cell death/proliferation state under irradiation. Cancer Lett 2002;182:217–22, doi:10.1016/S0304-3835(02)00079-4.
30. Cutrone JA, Yospur LS, Khalkhali I, et al. Immunohistologic assessment of technetium-99m-MIBI uptake in benign and malignant breast lesions. J Nucl Med 1998;39:449–53.
31. Fonti R, Salvatore B, Quarantelli M, et al. 18F-FDG PET/CT, 99mTc-MIBI, and MRI in evaluation of patients with multiple myeloma. J Nucl Med 2008;49:195–200, doi:10.2967/jnumed.107.045641.
32. Jia B, Shi J, Yang Z, et al. 99mTc-labeled cyclic RGDfK dimer: initial evaluation for SPECT imaging of glioma integrin alphavbeta3 expression. Bioconjug Chem 2006;17:1069–76, doi:10.1021/bc060055b.
33. Nomori H, Watanabe K, Ohtsuka T, et al. Evaluation of F-18 fluorodeoxyglucose (FDG) PET scanning for pulmonary nodules less than 3 cm in diameter, with special reference to the CT images. Lung Cancer 2004;45:19–27, doi:10.1016/j.lungcan.2004.01.009.
34. Balkwill F, Mantovani A. Inflammation and cancer: back to Virchow? Lancet 2001;357:539–45, doi:10.1016/S0140-6736(00)04046-0.
35. Rao VP, Poutahidis T, Ge Z, et al. Innate immune inflammatory response against enteric bacteria Helicobacter hepaticus induces mammary adenocarcinoma in mice. Cancer Res 2006;66:7395–400, doi:10.1158/0008-5472.CAN-06-0558.

Copyright of Molecular Imaging is the property of Decker Publishing and its content may not be copied or emailed to multiple sites or posted to a listserv without the copyright holder's express written permission. However, users may print, download, or email articles for individual use.